

PAPER • OPEN ACCESS

On wireless power transfer between coils in the presence of radiation

To cite this article: Ekaterina Shamonina *et al* 2021 *J. Phys. D: Appl. Phys.* **54** 405502

View the [article online](#) for updates and enhancements.

You may also like

- [Morphological characteristics and productivity of sugar palm saps at several levels of tapping age](#)
D K Wardani, A Junaedi, S Yahya et al.
- [Infrastructure performance of irrigation canal to irrigation efficiency of irrigation area of Candi Limo in Mojokerto District](#)
S Kisananto, R R R Hadiani and C Ikhsan
- [Improvement of the Ability of Representation, Reasoning, and Self-Efficacy of Prospective Mathematics Teacher Students by Using Learning with A Scientific Approach](#)
Darta, J Saputra, W Eliyarti et al.

On wireless power transfer between coils in the presence of radiation

Ekaterina Shamonina^{1,*} , Laszlo Solymar¹ and Victor Kalinin²

¹ University of Oxford, Department of Engineering Science, Parks Road, Oxford, OX1 3PJ, United Kingdom

² Transense Technologies plc, Bicester, Oxfordshire OX25 3SX, United Kingdom

E-mail: ekaterina.shamonina@eng.ox.ac.uk

Received 15 January 2021, revised 3 June 2021

Accepted for publication 17 June 2021

Published 20 July 2021



Abstract

Wireless power transfer (WPT) between magnetically coupled coils is necessarily accompanied by radiation that may hamper efficient power transfer and may cause harmful electromagnetic pollution. Hence careful control of the ratio between WPT and radiation is required. We have a formulation that allows the simultaneous determination of both the transferred and the radiated power by relying on both field and circuit theory and introducing the concept of a complex mutual inductance. Emphasis is placed on the visualisation of a radiative WPT system by using the streamlines of the Poynting vector. We perform several optimisations. We can find the parameters, coil radius, coil separation and load resistance, that maximise the ratio of load power to radiated power and at the same time minimise the radiated power. We identify the location of the singularities of the Poynting vector streamlines, the so-called P-points, and of the boundaries of a ‘power bubble’ surrounding the wireless two-coil system and forming an impenetrable barrier between the wireless power flow to the load and the power radiated out. A relationship between the size of the power bubble and the ratio between the useful load power and the harmful radiated power is established in a series of parametric studies. Field theory of Poynting vector streamlines is shown to quantitatively agree with the predictions of the circuit model. The new physical picture emerging for the power moving in space is expected to aid the design of complex practical WPT systems when radiation needs to be closely watched and for which a simple circuit model would fail to describe power distribution around the structure.

Keywords: wireless power transfer, Poynting vector streamlines, magnetic coupling, antennas, radiation, matching, magnetoinductive waves

(Some figures may appear in colour only in the online journal)

1. Introduction

Ever since the times of Marconi and Popov we had to face the dichotomy: wired or wireless. They had their own territories: wired mainly for telephone, wireless mainly for broadcasting. The balance was then tilted towards wireless with microwave

relays and satellite communications, and back again a little later to optical fibres. The successful assault of the wireless world came more recently with smart phones and they are now entering the tussle for power transfer. High power applications, e.g. charging car batteries, are still by wire and the same is true for domestic appliances like dishwashers and washing machines. However, for low power applications like charging mobiles, RFIDs, electric vehicles or wearables, wireless solutions are now a reality.

The usual configuration for wireless power transfer (WPT) is one transmitting coil that delivers power to one or more receiving coils. A problem that has not received due attention is that of concurrent radiation [1, 2]. Importantly, WPT and

* Author to whom any correspondence should be addressed.



Original Content from this work may be used under the terms of the [Creative Commons Attribution 4.0 licence](https://creativecommons.org/licenses/by/4.0/). Any further distribution of this work must maintain attribution to the author(s) and the title of the work, journal citation and DOI.

radiation are strictly interrelated. Both phenomena have been widely investigated in the last century or two. Coupled coils go back to Faraday's time, and radiation by dipoles has been studied since the beginning of the 20th century. However, these two physical phenomena were investigated independently of each other. It is the advent of circuit theory that made possible a connection between the two. By introducing radiation resistance it was possible to account for radiated power. Hence the two-coil problem could be solved by the following considerations: coil 1 is excited by an applied ac voltage that creates a current in coil 1. That current creates a magnetic field that induces a voltage in coil 2, which creates a current. This secondary current flows through a load resistance, an ohmic resistance and a radiation resistance which are then responsible for power transfer, ohmic losses, and radiation. This physical picture is very useful and appreciated by everyone who is involved with electrical engineering problems. It was widely used for analysis and optimisation of WPT between two coils [3–6] or several coupled coils [7–11]. The latter subject was closely linked with the new discipline of magnetoinductive waves which were born in the metamaterial context [12–15]. The radiation field on its own has been studied for well over a century, and there were many studies of the relationship between the near field and the far field. Alas most of these studies have been conducted in the context of antennas and little emphasis was given to the radiation field of near-field devices although with legal limits on the radiation strength these should also come into consideration. The usual practice is to treat the near field and far field separately, the former one concerned with WPT and the latter one with radiated power.

Efficient radiation is the function of every antenna, it is something desirable, but in the WPT context it is just a spurious effect that is harmful. A powerful method complementing the circuit analysis is to employ Poynting vector streamlines to visualise power flow using the field theory of Maxwell's equations. It's a technique that has been known for a long time and used in a large number of applications ever since its introduction in the 19th century. It can offer a useful alternative to the rays of geometric optics when studying such versatile near-field phenomena as design of holographic gratings [16], interaction of light with nanoparticles [17, 18], power transmission through subwavelength holes [19], subwavelength imaging using a multilayered 'superlens' [20, 21], power flow around receiving or transmitting antennas [22–26], coupling between circular coils in a conducting environment [27] or propagation of slow magnetoinductive waves via inter-element coupling in metamaterials [12, 13], to name a few. In the context of WPT, there has been a recent upsurge of interest to the Poynting vector streamlines method [28–32]. The questions addressed were the role of the load resistance [28], of variable receiver radius [30] or its lateral and angular misalignment [31] and power transfer in a multiple-coil domino system [32]. However all works considered only the near-field case that neglects radiation and focussed solely on near-field interactions.

A principal aim of this paper is to employ Poynting vector streamlines to expand our understanding of the power flow mechanisms in wireless systems when radiation cannot be neglected. We shall show that when radiation is taken

into account the Poynting vector streamlines offer a beautiful physical picture. They all originate in coil 1 and flow from there either to coil 2 following various paths or they tend towards infinity (also by various paths) accounting for radiation. Besides offering a new all-embracing physical picture the streamlines can also be used to determine the power relations. Those incident on coil 2 can be integrated over a suitably chosen surface to give the transferred power whereas an integration over a large radius in the far field gives the radiated power. Although we are certain about the superiority of the field model over the circuit model for seeing clearly the physical picture, we have no intention to discard the circuit model. We compare predictions based on the circuit model with those of the Poynting vector model confirming their full compatibility. The structure of this paper is as follows. In section 2, we invoke field theory to calculate electromagnetic fields and incorporate radiation into the circuit model of a WPT system of two magnetically coupled coils. Contrary to most treatments of WPT systems, we establish a relationship between radiation into the far field and the complex mutual inductance between the two coils of finite diameter. In section 3, we discuss optimisation scenarios for control of electromagnetic radiation and increase of WPT gain, evaluating the role of the internal resistance of the power source, the load resistance, the complex mutual inductance, ohmic losses in the coils as well as the coils' geometry. Section 4 presents Poynting vector visualisation for a variety of scenarios of interest in which WPT is accompanied by radiation, including the role of the load resistance, the geometry of the system and ohmic losses. Singularity points of the Poynting vector and the power 'bubble' surrounding the two-coils calculated from field theory are shown to be correlated with the predictions of the circuit model and the power relations from the circuit and the field model are proven to be in quantitative agreement. Conclusions are drawn in section 5.

2. WPT in the presence of radiation: field model and circuit model

We consider two magnetically coupled coils of radius a in the near field, arranged axially above each other at a distance d , as shown in figure 1(a). An alternating voltage V_1 of frequency ω is applied to coil 1 that excites a current I_1 in coil 1 and, by induction, a current I_2 in coil 2. We wish to determine the power delivered to the load in the second coil. In our theoretical calculations we shall take retardation into account, both for the far field and the near field, that leads necessarily to a complex mutual inductance between the two coils.

2.1. Field model

To find the electromagnetic fields produced by two coupled coils, we use the known expression for the vector potential $\mathbf{A} = A_\varphi \mathbf{i}_\varphi$ of a small circular coil carrying current I [33] and find the magnetic field \mathbf{H} from the relationship

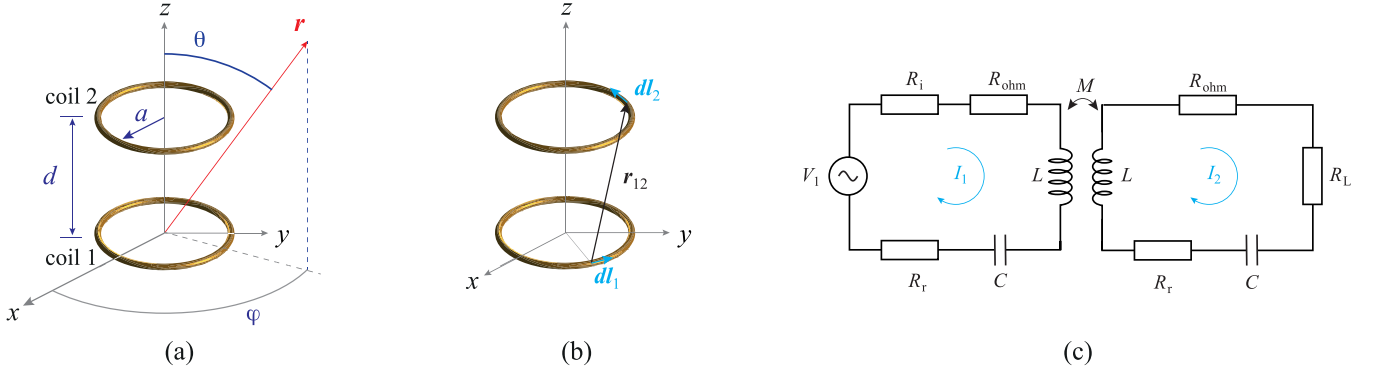


Figure 1. Schematic setup of two magnetically coupled coils arranged axially showing the spherical coordinate system (r, θ, φ) used in the field model (a) and showing quantities used to calculate the mutual inductance (b). The equivalent circuit of the system (c).

$$\mathbf{H} = \frac{1}{\mu_0} \nabla \times \mathbf{A} \quad (1)$$

where μ_0 is the permeability of vacuum. The corresponding electric field \mathbf{E} can be determined from Maxwell's equation. We do have the analytical expressions but often it is simpler to continue numerically.

Integrating the vector potential produced by coil 1 along coil 2 we can obtain the mutual inductance that will, contrary to usual Neumann integral approximation [34], contain both real and imaginary part,

$$M = \frac{\mu_0}{4\pi} \oint_{\text{coil 1}} \oint_{\text{coil 2}} \frac{e^{-jkr_{12}}}{r_{12}} \mathbf{dl}_1 \cdot \mathbf{dl}_2, \quad (2)$$

where $k = 2\pi/\lambda$ is the wavenumber, λ is the free space wavelength, \mathbf{dl}_1 and \mathbf{dl}_2 are infinitesimally small elements of coil 1 and coil 2, and the distance between them is r_{12} as illustrated in figure 1(b). This is a consequence of taking retardation into account, as discussed e.g. in [35, 36]. Oddly enough complex mutual inductance is hardly ever discussed in the literature although the related concept of mutual impedance (e.g. between dipole antennas) has been known and discussed for nearly a hundred years.

To calculate the radiation resistance of a coil carrying current I we shall find the radiated power. The Poynting vector

$$\mathbf{S} = \frac{1}{2} \text{Re}(\mathbf{E} \times \mathbf{H}^*) \quad (3)$$

simplifies in the far field to

$$\mathbf{S} = \frac{1}{2} \text{Re}(E_\varphi H_\theta^*) \mathbf{i}_r, \quad (4)$$

where asterisk denotes complex conjugation and \mathbf{i}_r is the unit vector in the radial direction. The total power radiated is given by the integral of the Poynting vector over a sphere sufficiently far away as

$$P_r = \frac{\pi\eta}{12} |I|^2 (ka)^4, \quad (5)$$

whence the well-known expression for the radiation resistance can be found as

$$R_r = \frac{\pi\eta}{6} (ka)^4 \quad (6)$$

where $\eta = 120\pi \Omega$ is the free space impedance.

When both coils radiate, the total electric field vector in the far field is given by [33]

$$E_\varphi = \frac{\eta k^2 a^2 \sin\theta}{4r} (I_1 + I_2 e^{-jkd \cos\theta}) e^{-jkr_1} \quad (7)$$

$$H_\theta = -\frac{1}{\eta} E_\varphi, \quad (8)$$

provided we neglect a structural scattering of the field from the coils.

2.2. Circuit model

The equivalent circuit for the two-loop system of figure 1(a) is shown in figure 1(c). The currents in coil 1 and coil 2 can be obtained from the relationship

$$\mathbf{V} = \mathbf{Z}\mathbf{I}, \quad (9)$$

which is a generalisation of Kirchhoff's equations [13]. In equation (9)

$$\mathbf{V} = \begin{pmatrix} V_1 \\ 0 \end{pmatrix}, \quad \mathbf{I} = \begin{pmatrix} I_1 \\ I_2 \end{pmatrix}, \quad \mathbf{Z} = \begin{pmatrix} Z_{11} & Z_{12} \\ Z_{21} & Z_{22} \end{pmatrix}. \quad (10)$$

The diagonal elements of the impedance matrix \mathbf{Z} are standing for the self-impedances of coils 1 and 2, which, assuming that the coils are at resonance with the series capacitances tuned in the absence of coupling, have the form

$$Z_{11} = R_i + R_{\text{ohm}} + R_r, \quad Z_{22} = R_L + R_{\text{ohm}} + R_r, \quad (11)$$

where R_i is the internal resistance of the voltage source, R_{ohm} is the ohmic resistance, R_r is the radiation resistance given by equation (6), and R_L is the load resistance in coil 2. The

off-diagonal elements of the impedance matrix stand for the mutual impedance,

$$Z_{12} = Z_{21} = j\omega M, \quad (12)$$

with

$$M = M_r + jM_i \quad (13)$$

being the complex mutual inductance given by equation (2). The ohmic resistance of each coil is quantified in our model by the quality factor, Q ,

$$Q = \frac{\omega L}{R_{\text{ohm}}}, \quad (14)$$

where L is the self-inductance of the coil. Solving equation (9), we obtain

$$I_1 = \frac{V_1 Z_{22}}{D}, \quad I_2 = -\frac{V_1 Z_{12}}{D}, \quad D = Z_{11} Z_{22} - Z_{12}^2. \quad (15)$$

2.3. Power relations

The purpose of the WPT system of figure 1 is to transfer power from coil 1 into coil 2 and keep the radiated power at minimum. From the circuit model, the power conservation implies that the input power

$$P_{\text{in}} = \frac{1}{2} \text{Re}(V_1 I_1^*). \quad (16)$$

is equal to the total output power,

$$P_{\text{out}} = \frac{1}{2} \text{Re} \left[\begin{pmatrix} I_1^* & I_2^* \end{pmatrix} \mathbf{Z} \begin{pmatrix} I_1 \\ I_2 \end{pmatrix} \right]. \quad (17)$$

Performing the matrix operations we obtain

$$P_{\text{out}} = \frac{1}{2} \text{Re} [Z_{11}|I_1|^2 + Z_{22}|I_2|^2 + Z_{12}(I_1 I_2^* + I_2 I_1^*)]. \quad (18)$$

The output power contains four contributions: the power delivered to the load in coil 2, P_T , the power radiated out by both coils, P_r , as well as the power dissipated on the internal resistance of the source, P_{R_i} , and in form of ohmic losses in both coils, P_{ohm} . As follows from equation (18), these power contributions can be written in the following form:

$$P_T = \frac{R_L}{2} |I_2|^2 \quad (19)$$

for the power delivered to the load,

$$P_r = \frac{R_r}{2} (|I_1|^2 + |I_2|^2) + \frac{1}{2} \text{Re} [Z_{12}(I_1 I_2^* + I_2 I_1^*)] \quad (20)$$

for the radiated power and

$$P_{R_i} = \frac{R_i}{2} |I_1|^2 \quad \text{and} \quad P_{\text{ohm}} = \frac{R_{\text{ohm}}}{2} (|I_1|^2 + |I_2|^2) \quad (21)$$

for the dissipated power on the internal resistance and for that due to ohmic losses in both coils, respectively.

2.4. An expression for the real part of the mutual impedance

Invoking again field theory, the radiated power can also be found by integrating over a spherical surface far away [37, 38],

$$P_r = \frac{R_r}{2} (|I_1|^2 + |I_2|^2) + \frac{\pi\eta}{2} (ka)^4 (I_1 I_2^* + I_2 I_1^*) f(kd), \quad (22)$$

where

$$f(kd) = \frac{\sin kd}{(kd)^3} - \frac{\cos kd}{(kd)^2}. \quad (23)$$

Assuming that there are no ohmic losses and no load resistance either, power can only be lost by radiation. It is given by equation (20) from the circuit model and by equation (22) from the field model. Equations (20) and (22) should now be identical. If they are identical that means that we can find the real part of the mutual impedance in two different ways, (a) from the radiated power using the far-field equations and (b) from Faraday's equation using the near-field values. We may find that

$$\text{Re}(Z_{12}) = -\omega M_i = \frac{\pi\eta}{2} (ka)^4 f(kd). \quad (24)$$

We have to emphasise how unusual is this result. Physical intuition and long-time practice tells us that mutual impedance is related to induced voltage hence it should be calculated from near-field equations, and from near-field equations alone. Here, in this very unusual case an analytical expression for the mutual inductance can be obtained from purely far-field considerations. A similar relationship was actually derived by Vendik a long time ago [39, 40] but somehow failed to cross the Iron Curtain. In fact, Vendik pointed out, that the imaginary part of the mutual impedance can also be determined without recourse to near-field equations by using the Kramers–Kronig [41] relations.

3. Power optimisation

Next we intend to find the optimum conditions. Following the WPT convention, we introduce the 'gain' quantities, defined as the ratio of a power quantity to the maximum available power $P_{\text{max}} = V_1^2 / (8 R_i)$:

$$g_{T,r,\text{ohm}} = \frac{P_{T,r,\text{ohm}}}{P_{\text{max}}}. \quad (25)$$

where subscripts T,r,ohm refer to the type of the power considered, transferred to the load, radiated or dissipated as ohmic loss, respectively. One possible optimisation aim could be to maximise the gain ratio g_T/g_r by varying R_L , a and d . There are no difficulties in doing it numerically. Unfortunately, the maximum comes when the distance between the coils and the coil radius tend to zero. That is obviously not what we want. We need a different approach. We should consider the distance between the coils and the operating frequency as fixed parameters, i.e. as constraints likely prescribed by the requirements of a practical WPT system. We also fix the values of the

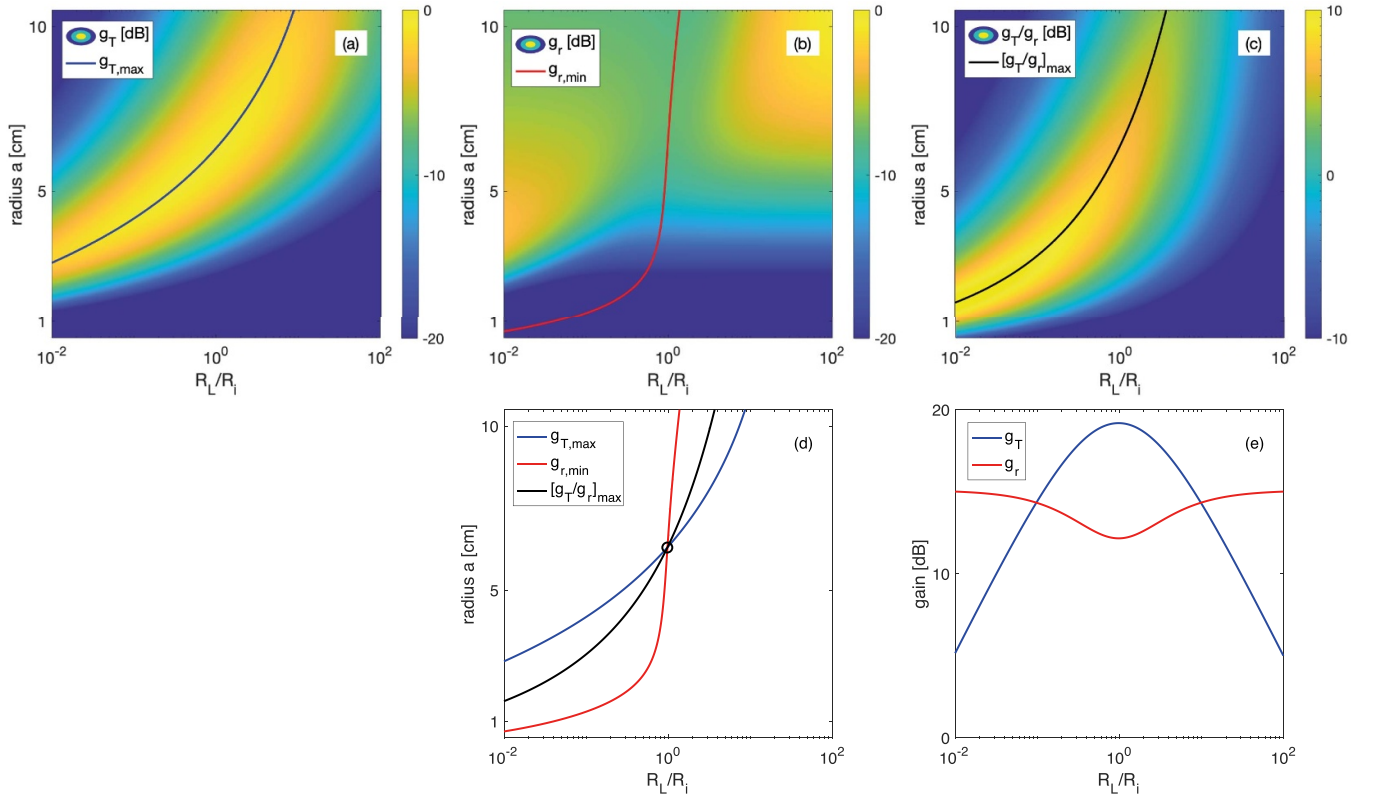


Figure 2. Gain variation with load resistance and coil radius for (a) load power, (b) radiated power and (c) their ratio. Distance between coils $d = 8$ cm, $\lambda = 1$ m, lossless case. Solid curves show the optimum load resistance optimising each of the gain quantities at every coil radius. (d) Three optimum load curves with their crossing point giving the optimum radius. (e) Variation of the load gain and radiated power gain with load resistance at the optimum radius confirming the optimum load for the three-fold optimisation of (a)–(c).

internal resistance, R_i , and the quality factor, Q , as these are not free optimisation parameters either. We can then proceed with the maximisation of g_T/g_r , in terms of only two free parameters, load resistance, R_L and coil radius, a . However there is one more problem to solve. g_T/g_r might be maximum for the given parameters but the corresponding load power might still be small. Hence what we need is to do a threefold optimisation. Choose all the parameters except the load resistance and the coils radius and then vary those two quantities to find the minimum of radiated power, maximum of load power and also the maximum of their ratio. This turns out to be possible.

Let us first consider as an example a lossless case, $Q = \infty$. Figures 2(a)–(c) show, as contour plots, variation of three quantities of interest, gains g_T , g_r , and their ratio g_T/g_r against load resistance R_L and coil radius a for $\omega/(2\pi) = 300$ MHz (i.e. $\lambda = 1$ m), $d = 8$ cm, $R_i = 50 \Omega$.

As seen from figure 2(a), there is an optimum load resistance for every coil radius (and hence for the corresponding values of M and R_r), that maximises the power delivered to the load. This optimum load resistance can be found analytically from equation (19) as

$$R_{L,\max} = \sqrt{R_\Sigma^2 + 2 \frac{R_\Sigma \delta^2}{Z_{11}} + \frac{\gamma^4}{Z_{11}^2}}. \quad (26)$$

where the notations $R_\Sigma = R_r + R_{\text{ohm}}$, $\delta^2 = \beta^2 - \alpha^2$, $\gamma^2 = \beta^2 + \alpha^2$, $\alpha = \omega M_i$ and $\beta = \omega M_r$ are introduced for convenience.

This variation of the optimum load with the coil radius is shown in figure 2(a) as a blue curve. We note that this optimum is strongly affected by the chosen value of the internal resistance of the voltage source, R_i .

In figure 2(b), we perform a different optimisation, looking this time for the optimum load value that minimises the radiation for any chosen geometry, shown as a red curve. This optimum load value can be found from equation (20) in its analytical form as

$$R_{L,\min} = \frac{-B + \sqrt{B^2 - 4AC}}{2A} - R_\Sigma \quad (27)$$

where

$$A = \alpha^2 Z_{11}^2 + \delta^2 R_r Z_{11}, \quad B = R_r \gamma^2 (\gamma^2 - Z_{11}^2), \quad C = -\alpha^2 \gamma^4 - \delta^2 \gamma^2 R_r Z_{11}. \quad (28)$$

We note that this optimum is also strongly affected by the chosen value of R_i .

In figure 2(c), we perform a third type of optimisation, finding optimum load for the gain ratio g_T/g_r . From equations (19) and (20) this optimum load is found as

$$R_{L,\text{opt}} = \gamma \sqrt{1 + \frac{R_\Sigma^2}{\gamma^2} - 2 \frac{R_\Sigma}{R_r} \frac{\alpha^2}{\gamma^2}} \quad (29)$$

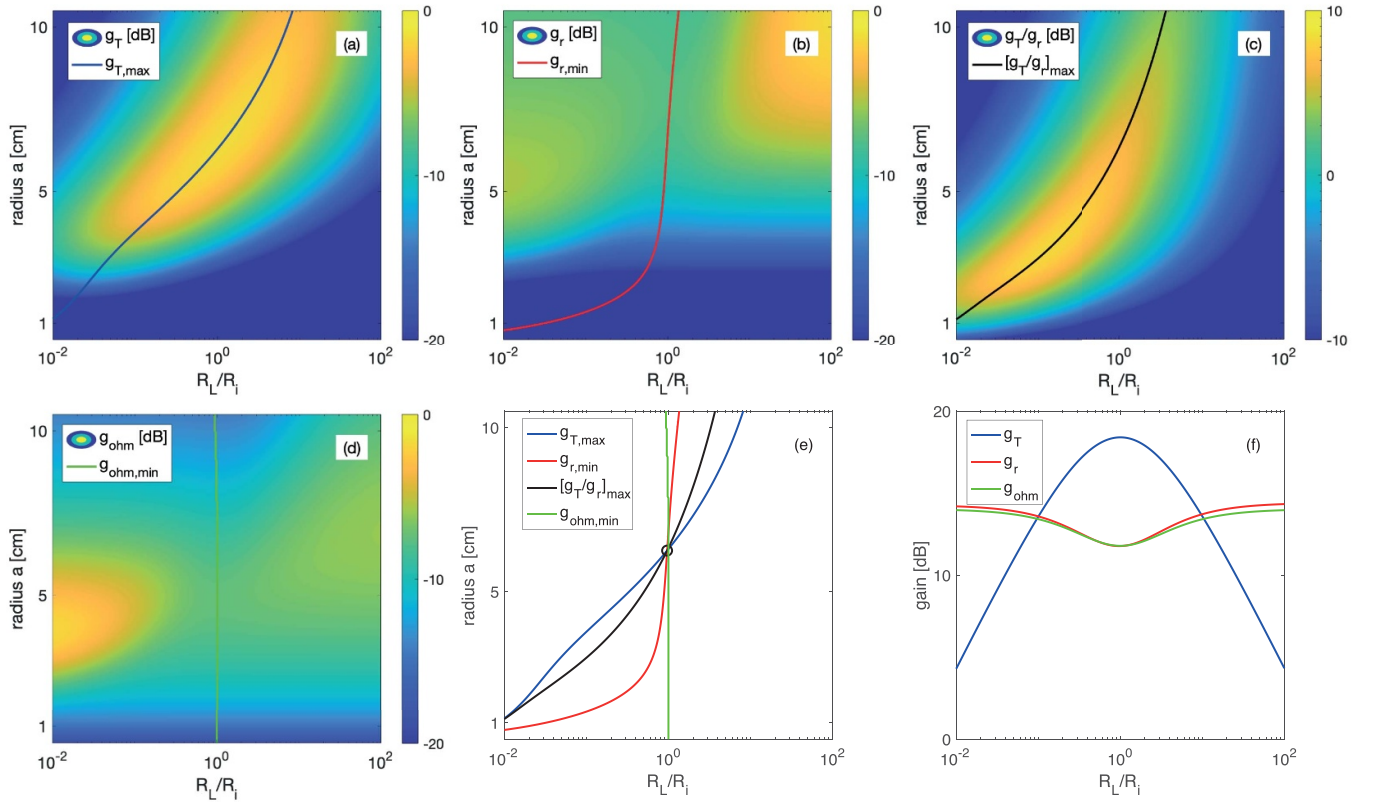


Figure 3. Same as figure 2 but with ohmic losses included. Gain variation with load resistance and coil radius for (a) load power, (b) radiated power, (c) their ratio and (d) ohmic losses. Distance between coils $d = 8$ cm, $\lambda = 1$ m, $Q = 150$. Solid curves show the optimum load resistance optimising each of the gain quantities at every coil radius. (e) Four optimum load curves with their crossing point giving the optimum radius. (f) Variation of the load gain and radiated power gain with load resistance at the optimum radius confirming the optimum load for the four-fold optimisation of (a)–(d).

and visualised in figure 2(c) by a black curve. We note that this optimum load is independent of the value of the source internal resistance.

As follows from equations (26), (27) and (29), we can simultaneously optimize power transfer to the load and minimize the total radiated power if we manage to select the coupling in such a way that $R_{L,max} = R_{L,min} = R_{L,opt}$. In figure 2(d), all three optimisations are shown in the same plot, with their crossing point (marked as a circle) yielding the optimum conditions that would maximise the power delivered to the load and minimise the power radiated out. This is confirmed by figure 2(e) presenting the variation of the transferred and radiated power with R_L for this optimum configuration which, for the chosen distance $d = 8$ cm and $R_i = 50 \Omega$, gives optimum radius of coils as $a = 6.3$ cm that corresponds to $\omega M = (47.9 - 4.4j) \Omega$. The resulting optimum load resistance is $R_L = 48.2 \Omega$.

In figure 3, we repeat the same exercise, but this time using a relatively large value of ohmic losses, taking $Q = 150$, and keeping other parameters unchanged. The structure of the plots is identical to those in figure 3, except there are now four contour plots shown, adding also g_{ohm} to our set of the gains. Optimisation of all four quantities is shown in figure 3(e) allowing for similar conclusions as in the lossless case, whereas figure 3(f) illustrates that, at the optimum radius,

the optimum load resistance results in maximising the load power while simultaneously minimising radiative and ohmic losses. The effect of ohmic losses can be appreciated by comparing figure 2 (lossless) and figure 3 (lossy). Clearly the overall gain values are affected by the ohmic losses, but there are no major effects to notice. Interestingly, the ohmic losses can be seen to compete with the radiative losses. The radiation can be clearly seen to be suppressed at low load values and at the radius near 5 cm when ohmic losses are included (cf figures 2(b) and 3(b)) which is indeed the range of parameters when ohmic losses are dominant (see figure 3(d)). We conclude that for the chosen range of parameters ohmic losses do not play a major role in the interplay between the load gain and the radiation gain.

Performing the above three-fold optimisation for different values of distance d , we extract for each of the configurations the optimum radius, the corresponding values of the gain quantities as well as the impedance quantities (load resistance, radiation resistance and mutual inductance). These results are summarised in figure 4. Solid lines are for the lossless case and dashed lines are for $Q = 150$. Figure 4(a) shows the optimum radius versus the distance between coils, figure 4(b) shows the optimised gain quantities g_T (blue), g_r (red), and, in the lossy case, g_{ohm} (green) as a function of the distance between coils. These values of the gain are calculated for the optimum load

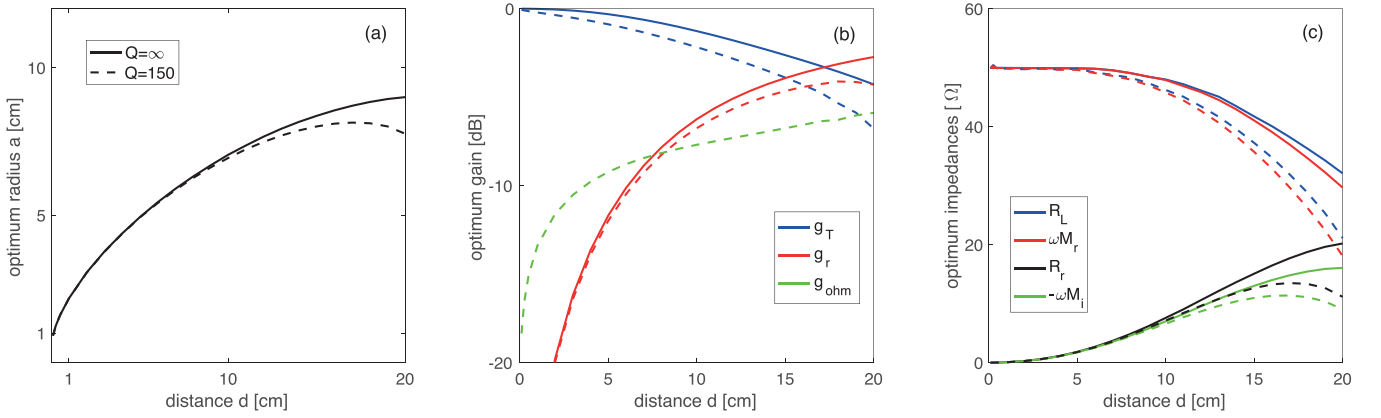


Figure 4. Variation of the optimised setup with distance: (a) optimum radius, (b) gain for load power, radiated power and ohmic losses and (c) the corresponding load resistance, mutual impedance and radiation resistance. Solid curves: lossless case, dashed curves: $Q = 150$.

resistance R_L , which is shown in figure 4(c) (blue), together with three further impedance quantities, ωM_r (red), R_r (black) and ωM_i (green). The difference between the solid and the dashed lines illustrates the effect of the ohmic losses, which, for the considered set of parameters, is quite moderate.

As seen from figure 4(a), the geometric aspect ratio a/d decreases with the distance between the coils due to the radiation effect, from 9 for $d = 1$ mm to 1 for $d = 5$ cm, to 0.4 for $d = 20$ cm in the lossless case. This makes sense: a simple scaling of a with d would result in a suboptimal performance for power transfer due to radiation becoming too strong. When ohmic losses are included, the decrease of the aspect ratio a/d with d becomes even stronger and the optimum radius does not increase beyond 8 cm.

The optimum gain variation with distance in figure 4(b) reflects the expected deterioration of the gain ratio with increased size of the structure. In figure 4(c), we can note that for smaller structures, such that $M_i \ll M_r$, $R_r \ll \omega M_r$ and $R_i \gg R_r$, a simple matching condition holds true, $R_L \approx \omega M_r \approx R_i$. It is worth noting that the value of ωM_r being the characteristic impedance of the lossless magnetoinductive waveguide was derived some 20 years ago in the context of magnetoinductive waves [13]. However, for larger structures, the deviation of the optimum load resistance from ωM_r and from R_i becomes quite significant.

4. Poynting vector streamlines, ‘power bubbles’ and singularity points

It is not particularly difficult to envisage WPT from one coil to another coil. The physical picture is clear. An a.c. voltage creates a current in the first coil that creates a time-varying magnetic field, that crosses the second coil and induces thereby a voltage in the second coil. The induced voltage then creates a current in the load resistance of the second coil. We can distinguish five different physical phenomena. (a) Applied voltage creates current, (b) current creates magnetic field, (c) magnetic field induces voltage, (d) induced voltage creates current, (e) current is absorbed in the load, and that completes the power transfer. Another way of envisaging power transfer is much

simpler, much more direct, appeals much more to the senses but, oddly enough, not very often used. They are the Poynting vector streamlines. In this section we aim to provide insights into the mechanisms of WPT in the presence of radiation visualising the optimisation mechanisms discussed.

An important remark is that the Poynting vector calculated from the field model shows what happens to the power once it has been emitted by coil 1. The shape of the Poynting vector streamlines for the two-coil geometry of figure 1 is uniquely defined by four parameters only: three geometric ones, namely, the wavelength, λ , the radius of the coils, a , and the distance between them, d , and by the fourth one: the current ratio I_2/I_1 . As follows from equation (15),

$$\frac{I_2}{I_1} = \frac{j\omega M}{R_L + R_{ohm} + R_r}, \quad (30)$$

so that the power streamlines are entirely independent of the source internal resistance or the amplitude of the source voltage. Moreover, for any chosen geometry, M , R_r and R_{ohm} are constant and the only parameter that will determine the way power can flow is the load resistance R_L . As Poynting vector streamlines do not depend on the source voltage or internal resistance, we will normalise the amplitude of the Poynting vector so that total power emitted by the transmitter coil, $P_L + P_{ohm} + P_r$, will be 1 W. By analysing the streamlines and the amplitude of the Poynting vector we aim to visualise the physical mechanisms of the power flow.

4.1. Mismatched load

To provide a point of reference, let us first look at the case when retardation is neglected and we have only transfer of power to the load. This case was studied in the past in the context of non-radiative power transfer by means of magnetoinductive waves [12, 13]. This is shown in figure 5(a) for the lossless case with $\lambda = 1$ m, $d = 8$ cm, $a = 4$ cm. Without radiation, only transfer of power from coil 1 to coil 2 can take place. The streamlines are shown in the xz plane, but due to the rotational symmetry of the structure the same picture would emerge in any plane containing the axis of the symmetry, the

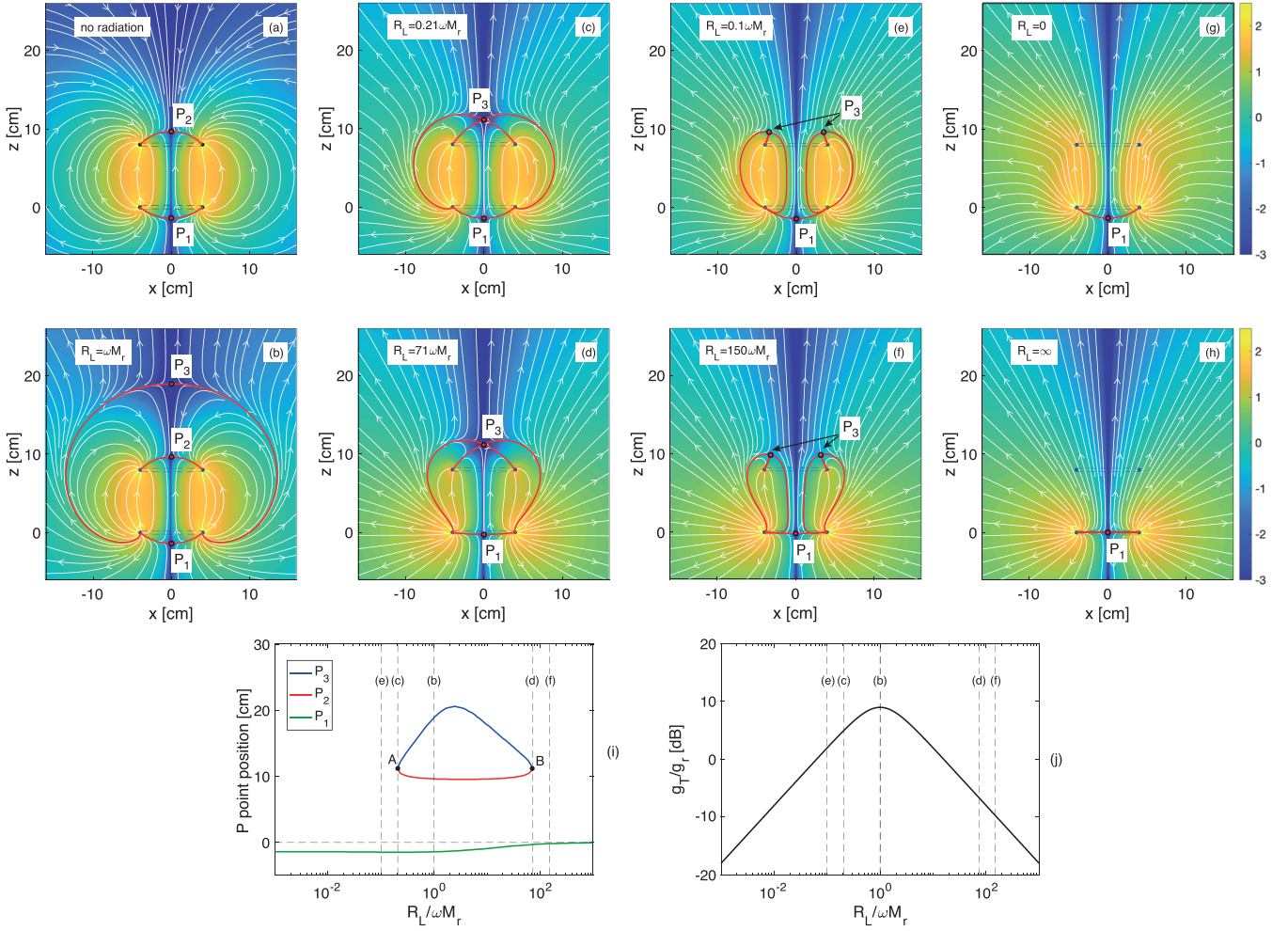


Figure 5. Role of the load resistance. Poynting vector \mathbf{S} streamlines and magnitude for a two-coil system with $a = 4$ cm and $d = 8$ cm. (a) No radiation; (b)–(h) with retardation, for different load values: $R_L/(\omega M_r) = 1$ (b); 0.21 (c), 71 (d), 0.11 (e), 150 (f), 0 (g) and ∞ (h). Location of the singularity points is labeled as P_1 , P_2 and P_3 . Poynting vector magnitude is normalised to yield total power emitted by transmitter to be 1 W. (i) Positions of the singularity P-points and (j) load/radiation gain ratio versus load resistance.

z axis. It may be seen that all the streamlines originate on coil 1, and all of them terminate on coil 2. The Poynting vector has two singularities (its value is zero) in two so-called P-points [13, 23, 25], one below the first coil and the other one above the second coil, which we denote as P_1 and P_2 . The red lines separate two families of streamlines, those moving from coil 1 to coil 2 via inside the cylinder and those moving via outside the cylinder (the cylinder is defined by the two coils). There is of course a trivial case along the axis of the structure (not shown) where due to symmetry the Poynting vector is zero and which, in any plane, would separate the power that flows ‘to the left’ of the symmetry axis from power that flows to the ‘right’. The singularity points P_1 and P_2 form when the boundaries of the separating families cross and Poynting vector singularities of this kind have been observed in a variety of other physical phenomena when an antenna or a metallic object was receiving power [17, 19, 23, 25, 26].

Next, we shall look at the case when there is radiation. The family of seven plots shown in figures 5(b)–(h) illustrates the role of the mismatch in the load resistance, R_L . Ohmic

losses are not included in this example to highlight the interplay between the load power and the radiated power.

Figure 5(b) is for $R_L = \omega M_r$, that provides the optimum power ratio between the power delivered to the load and the power radiated out. The streamlines in figure 5(b) very close to the structure look quite similar to those in figure 5(a). Two singularity points, P_1 and P_2 , are at about the same place but there is one major difference. In figure 5(a), the streamlines above coil 2 move downwards descending upon coil 2. In figure 5(b) some of the streamlines above coil 2 move also upwards out to infinity. There is now a third singularity point, P_3 , in figure 5(b) that divides the streamlines that radiate out, from those which descend upon coil 2 from above. There are now three families of streamlines, those that reach coil 2 via the inside, those that reach coil 2 via the outside and those that radiate out, with the red lines showing the boundaries between them. A complete bubble can be seen to have formed that surrounds the system of two coils. This ‘bubble’ is a new feature and is characteristic to all the cases when there is power transfer to the second coil in the presence of retardation.

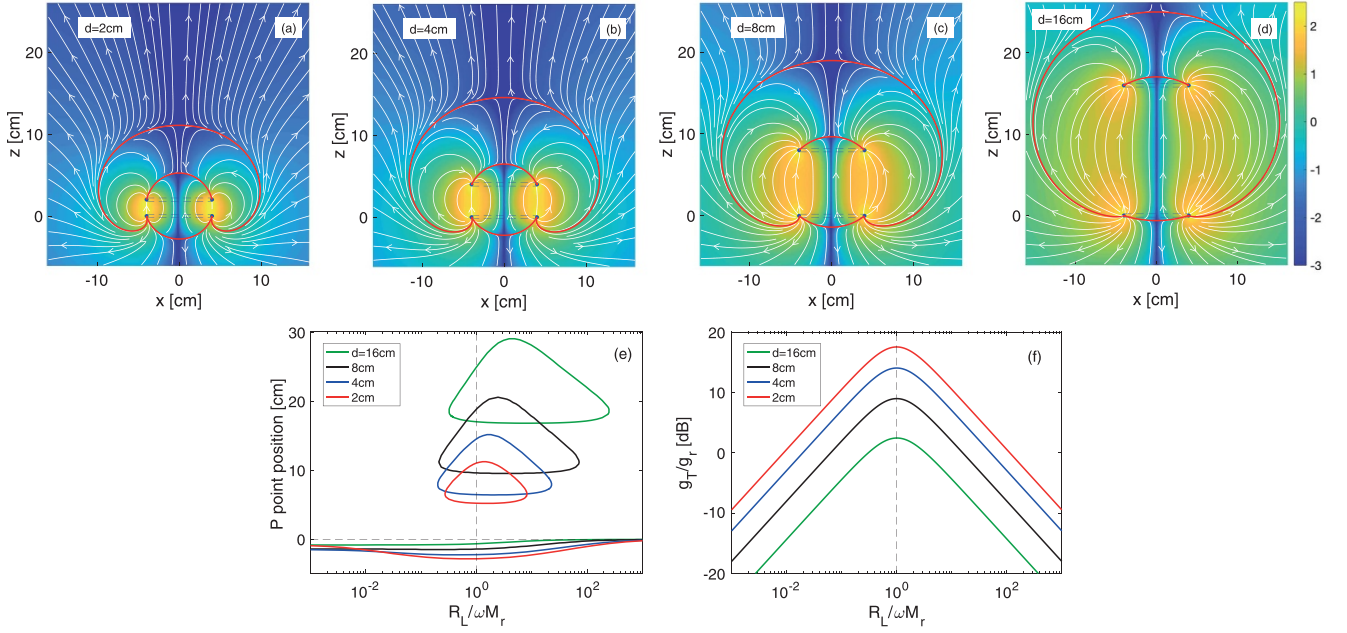


Figure 6. Role of the distance. Poynting vector \mathbf{S} streamlines and magnitude for a two-coil system with $a = 4$ cm for different distance values: (a) $d = 2$, (b) 4, (c) 8 and (d) 16 cm. Lossless case. Poynting vector magnitude is normalised to yield total power emitted by transmitter to be 1 W. (e) Positions of the singularity P-points and (f) load/radiation gain ratio versus load resistance.

In figures 5(c) and (d), we show two cases, one below the other, when a mismatched load is either too small, $R_L = 0.21 \omega M_r$ (c), or too large, $R_L = 71 \omega M_r$ (d). From our circuit model, we expect a deterioration for the load/radiation power ratio. In both cases, the singularity point P_1 below coil 1 is still there, but the singularities P_2 and P_3 above coil 2 merge now into a single point. The power ‘bubble’ shrinks in comparison to figure 5(b), indicating a less efficient power transfer and a more significant radiation.

Figures 5(e) and (f) show two cases (again, one below the other one) of even more severely mismatched load, $R_L = 0.1 \omega M_r$ (e) and $R_L = 150 \omega M_r$ (f). There is now considerable difference in the shape of the surface shown in red. It is no longer a closed bubble. It turns into a doughnut that is separating the power flow to coil 2 and the power radiated out. The singularity P_1 below coil 1 is present. Interestingly, the singularity above coil 2 that was in the previous examples positioned on the axis of the symmetry appears now off axis as two symmetric P-points. Due to the rotational symmetry of the geometry, it is clear that this singularity point has now transformed into a singularity ring. Notice that in these cases of a severely mismatched load, part of the radiation moves via the inside of the cylinder formed by both coils, i.e. passing through the doughnut’s hole before radiating out.

The most severely mismatched cases are figure 5(g) with zero load and figure 5(h) with infinite load. In both cases there is no power transfer to the load, with all power radiating out. The difference between the two cases is that when $R_L = 0$ current can pass through coil 2, only to contribute to the radiation, but when $R_L = \infty$ no current can pass through coil 2, which may be seen to be transparent to the power flow. In both cases (g) and (h), there is a singularity point near coil 1 that

separates the streamlines moving respectively downwards and upwards (or, moving via the outside or via the inside the cylinder formed by both coils). As may be seen there is no power transfer to coil 2.

As illustrated in figures 5(b)–(h), the volume of the power bubble serves as a good indicator for the ability of the load gain to suppress the radiated gain. A large volume of the power bubble for a chosen geometry correlates strongly with the load/radiated gain ratio being near optimum. Another good indicator for the increase in radiation for a mismatched load is the amplitude of the power density shown by colour of the contour plots for $|\mathbf{S}|$. One clearly visible feature is that outside the power bubble difference in colour (more of the blue in the matched case (b), more of the yellow/green in the mismatched cases (h)) quantifies that radiation is indeed more suppressed in the matched case.

Summarising the streamline results, we show in figure 5(i) the positions of the three P-points as a function of the load resistance and figure 5(j) the corresponding gain ratio g_T/g_r . The vertical dashed lines in both graphs (i) and (j) identify the configurations shown in subplots (b)–(f). Points A and B in figure 5(i) (corresponding to the cases of figures 5(c) and (d)) are special cases. This is where the singularity points P_3 and P_2 merge, one for mismatch by a smaller load (point A) and the other one for mismatch by a bigger load (point B). For load resistance lower than in point A or larger than in point B, the power bubble transforms into a doughnut, the singularity points P_2 and P_3 transform into singularity rings and the power can radiate not only outside the doughnut but also through the doughnut hole. The lower singularity point P_1 exists for all values of the load resistance.

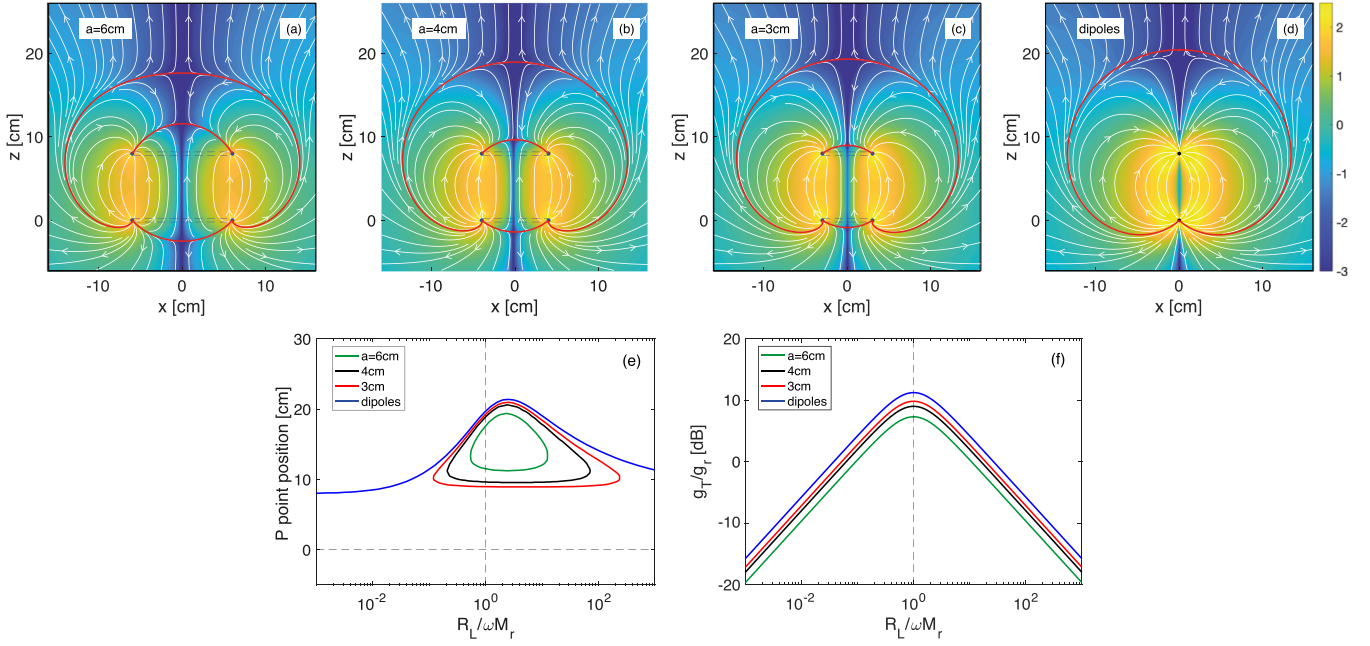


Figure 7. Role of the radius. Poynting vector \mathbf{S} streamlines and magnitude for a two-coil system with $d = 8$ cm for different distance values: (a) $a = 6$, (b) 4, (c) 3 cm and (d) dipole model. Lossless case. Poynting vector magnitude is normalised to yield total power emitted by transmitter to be 1 W. (e) Positions of the singularity P -points and (f) load/radiation gain ratio versus load resistance.

4.2. Varying geometry

In the next two examples we visualise the role of the geometry on the radiation. Using the matched load resistance in each case, in the four plots of figures 6(a)–(d) the Poynting vector is shown for the configurations in which the radius is kept constant at $a = 4$ cm, but the distance increases from 2 cm to 16 cm. It can be clearly seen that the radiation increases for a larger structure, and a clear ‘leakage’ of the power below the power bubble for a larger structure of figure 6(d) provides a clear contrast to the case (a) where very low electromagnetic radiation is present with most power delivered safely to the load. Similar to the previous figure, in plots (e) and (f) we show the positions of the singularity points as a function of the load resistance and the corresponding gain ratio g_T/g_r for the four geometries considered in plots (a)–(d). The position of the lowest singularity point (labeled as P_1 in figure 5(i)) can be seen to be affected very little by the changes in the geometry. The power bubble is intact at the optimum load, the gain ratio deteriorates with the increased distance, matching our expectations from the circuit model. We note that figure 6(c) is identical with figure 5(b): this is the reference case of the matched load with $a = 4$ cm and $d = 8$ cm.

Similarly, in the four plots of figures 7(a)–(d) we look at four configurations in which the distance is kept constant at $d = 8$ cm, but the radius decreases. The first three examples shown are for $a = 6, 4$, and 3 cm. The fourth example shows the case of two magnetic dipoles calculated using standard formulas [33] which could also be derived from our model in the limiting case $a \rightarrow 0$. Figure 7(e) shows the positions of the top singularity points of the Poynting vector as a function of the load resistance and figure 7(f) the corresponding gain ratio g_T/g_r for the four geometries considered in plots (a)–(d). P_1

point position changes very little (not shown). The physical picture matches the predictions of the circuit model. Radiation is clearly suppressed when the radius is smaller. This is also confirmed by the range of the load values for which the top singularities P_2 and P_3 exist, i.e. for which the power bubble remains intact. For a smaller radius, the power that travels via the inner part of the cylinder formed by both coils cannot escape and will end up on coil 2, contributing to the load power, even when the load is mismatched. For two dipoles this is the case for any load value.

4.3. Ohmic losses

So far we did not include ohmic losses when looking at the Poynting vector streamlines. Power dissipated as ohmic losses in coil 1 does not show up in streamlines emitted by the coil, and there is no direct way to discriminate between the power flow that will be dissipated as ohmic losses on coil 2 and the power flow that will be delivered to the load, also in coil 2. In the Poynting vector streamline picture both types of power are contained within the power bubble. We can however draw meaningful conclusions by comparing the lossless and the lossy case. In figures 8(a) and (b), we show the changes caused by ohmic losses to the singularity points of the Poynting vector and to the gain ratio for the same reference geometry with $a = 4$ cm and $d = 8$ cm. We use four values of the quality factor, a lossless case (black curves), $Q = 500$ (red curves), 200 (blue curves) and 150 (green curves). As clearly seen the changes caused by ohmic losses are mild. The amount of ohmic losses for the considered configuration is not a dominant contribution in comparison to the radiation. The most interesting feature seen in plot (a) is that, for lower Q values, the

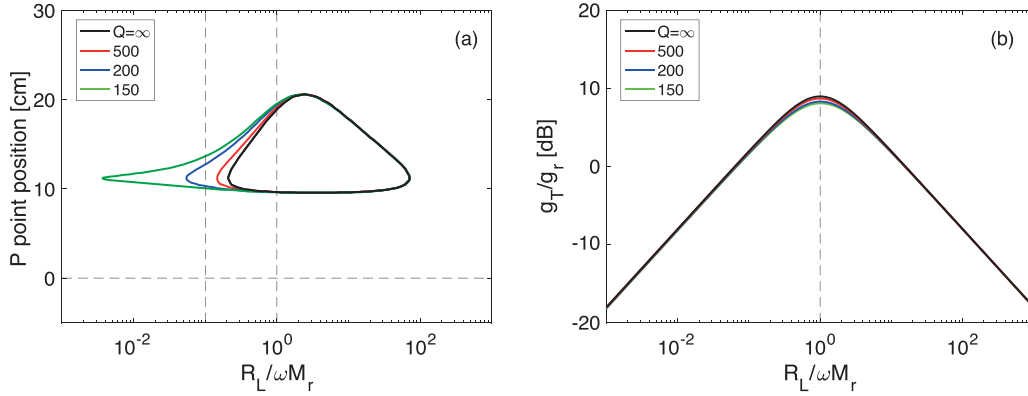


Figure 8. Role of ohmic losses. (a) Positions of the singularity P-points and (b) load/radiation gain ratio versus load resistance for different values of the quality factor.

Table 1. Power quantities (in mW) calculated from the circuit and the field model.

	Circuit model	Field model
P_{in}	39.61	39.57
P_r	4.39	4.39
P_T	35.22	35.18

power bubble remains intact even for a severely mismatched load, when load resistance is way below the optimum value. The physical explanation is that ohmic losses are a competing mechanism to the radiation. By increasing the ohmic losses, this mechanism enhances and the power bubble stays intact as the power that travels via the inside ends up on coil 2.

4.4. Power conservation

Finally, we shall look at power relations, as obtained by the circuit approach and field approach respectively. The two should of course agree but considering the number of approximations used in the analysis, it cannot be taken for granted. It needs to be shown because otherwise the results cannot be fully trusted. The expressions for the power delivered to the load and for the radiated power were given by the circuit approach as equations (19) and (20). To determine the same powers by the field approach we shall rely on our Poynting vector calculations.

First the radiated power. It can be easily obtained numerically by integrating the Poynting vector over a sufficiently large sphere surrounding the coils. To find the power leaving coil 1, i.e. the input power, we need a more complicated arrangement. We shall assume a toroid that encloses coil 1, and then integrate the normal component of the Poynting vector, pointing everywhere outwards, over that surface. For finding the transferred power we can follow the same procedure assuming a toroid enclosing coil 2 and integrating the Poynting vector which will now point inwards.

For the power calculations we shall assume the following parameters: $a = 4$ cm, $d = 8$ cm, $R_L = 12.458 \Omega$, $R_r = 0.777 \Omega$, $M_i = -0.40$ nH, $M_r = 6.61$ nH. $V_1 = 1$ V. The quantities, P_{in} , P_r , and P_T as calculated for the above parameters,

are shown in table 1 for the circuit and field models, respectively. The largest deviation between them occurs for P_T where it amounts to 0.11%.

Interestingly, a simple estimate of the power radiated and power delivered to the load can also be obtained by analysing the ‘projectile exit angles’ of two power bubble lines shown in figure 5: one leaving loop 1 towards the singularity point P_1 and another one towards the singularity point P_3 . This analysis (not shown here) is found to be in qualitative agreement with the more rigorous calculations presented here confirming the usefulness of the Poynting vector analysis for the problem of WPT in the presence of radiation. We expect that this approach will be valuable in provide a physical picture of power distribution around more complex WPT systems.

5. Conclusions

A detailed study of two coupled coils has been undertaken by relying on a model that can simultaneously take into account both power transfer between the coils and radiation effects. We have used both a field approach and a circuit approach whose results are compared and shown to be very close (of the order of 0.1%) to each other. We have found the load resistance that can maximise power transfer and at the same time minimise the radiated power.

The field approach leads directly to a formulation in terms of the streamlines of the Poynting vector. To the best of our knowledge, this study is the first time when a radiative WPT system is visualised using the Poynting vector formulation. A detailed investigation of these streamlines reveals an up-to-now unknown physical picture showing how the transferred and radiated power move in space depending on the choice of the parameters. Plotting the streamlines of the Poynting vector is not only the best visual means of seeing the electromagnetic power, literally, moving, but in our case the simplest as well.

We have established a clear correlation between the ratio of the transmitted and radiated power and the position of the singularity P-points for the streamlines, and the volume of the power ‘bubble’ enclosing the space within which the power is delivered to the load. Role of the load resistance, of the

geometry of the coils and of ohmic losses are studied. Streamlines of the Poynting vector are shown to enhance our understanding of the physical processes that can be used as a tool aiding the design of complex practical WPT systems when radiation cannot be neglected and for which a simple circuit model would fail to describe power distribution around the structure.

Data availability statement

The data that support the findings of this study are available from the authors upon reasonable request.

Acknowledgment

ES would like to acknowledge financial support by the EPSRC UK (SYMETA Grant EP/N010493/1).

ORCID iD

Ekaterina Shamonina  <https://orcid.org/0000-0002-0269-7273>

References

- [1] Faria J A B 2012 Poynting vector flow analysis for contactless energy transfer in magnetic systems *IEEE Trans. Power Electron.* **27** 4292–300
- [2] Li L, Dai H, Chen G, Zheng J, Dou W and Wu X 2019 Radiation constrained fair charging for wireless power transfer *ACM Trans. Sens. Networks* **15** 1–33
- [3] Kurs A, Karalis A, Moffatt R, Joannopoulos J D, Fisher P and Soljačić M 2007 Wireless power transfer via strongly coupled magnetic resonances *Science* **317** 83–6
- [4] Karalis A, Joannopoulos J D and Soljačić M 2008 Efficient wireless non-radiative mid-range energy transfer *Ann. Phys.* **323** 34–48
- [5] Imura T and Hori Y 2011 Maximizing air gap and efficiency of magnetic resonant coupling for wireless power transfer using equivalent circuit and Neumann formula *IEEE Trans. Ind. Electron.* **58** 4746–52
- [6] Fu M, Yin H, Zhu X and Ma C 2015 Analysis and tracking of optimal load in wireless power transfer systems *IEEE Trans. Power Electron.* **30** 3952–63
- [7] Cannon B L, Hoburg J F, Stancil D D and Goldstein S C 2009 Magnetic resonant coupling as a potential means for wireless power transfer to multiple small receivers *IEEE Trans. Power Electron.* **24** 1819–25
- [8] Zhang F, Hackworth S A, Fu W, Li C, Mao Z and Sun M 2011 Relay effect of wireless power transfer using strongly coupled magnetic resonances *IEEE Trans. Magn.* **47** 1478–81
- [9] Solymar L and Shamonina E 2011 Optimal power transfer by coupled resonant coils *Proc. 5th Int. Congress on Advanced Electromagnetic Materials in Microwaves and Optics (Metamaterials 2011) (Barcelona, Spain)* pp 18–20
- [10] Kiani M and Ghovanloo M 2012 The circuit theory behind coupled-mode magnetic resonance-based wireless power transmission *IEEE Trans. Circuits Syst.* **59** 2065–74
- [11] Hui S Y R, Zhong W and Lee C K 2013 A critical review of recent progress in mid-range wireless power transfer *IEEE Trans. Power Electron.* **29** 4500–11
- [12] Shamonina E, Kalinin V A, Ringhofer K H and Solymar L 2002 Magneto-inductive waveguide *Electron. Lett.* **38** 371–2
- [13] Shamonina E, Kalinin V A, Ringhofer K H and Solymar L 2002 Magnetoinductive waves in one, two and three dimensions *J. Appl. Phys.* **92** 6252–61
- [14] Syms R R A, Shamonina E and Solymar L 2006 Magneto-inductive waveguide devices *IEE Proc. Microw. Antennas Propag.* **153** 111–21
- [15] Syms R R A, Sydoruk O, Shamonina E and Solymar L 2007 Higher order interactions in magneto-inductive waveguides *Metamaterials* **1** 44–51
- [16] Russell P S J 1981 Thick grating focussing-device-design using Poynting-vector-optics *Appl. Phys. B* **26** 37–42
- [17] Bohren C F 1983 How can a particle absorb more than the light incident on it? *Am. J. Phys.* **51** 323–7
- [18] Wang Z B, Lukyanchuk B S, Hong M H, Lin Y and Chong T C 2004 Energy flow around a small particle investigated by classical Mie theory *Phys. Rev. B* **70** 035418
- [19] Stavrinou P N and Solymar L 2002 The propagation of electromagnetic power through subwavelength slits in a metallic grating *Opt. Commun.* **206** 217–23
- [20] Shamonina E, Kalinin V A, Ringhofer K H and Solymar L 2001 Imaging, compression and Poynting vector streamlines for negative permittivity materials *Electron. Lett.* **37** 1243–4
- [21] Liu Z, Lee H, Xiong Y, Sun C and Zhang X 2007 Far-field optical hyperlens magnifying sub-diffraction-limited objects *Science* **315** 1686
- [22] Müller B 1972 Energy flow in the near field of a receiving antenna *AEÜ* **26** 443–9
- [23] de la Fuente P 1976 The singularities of the time-averaged flow of electromagnetic energy *Nachr. Tech. Z.* **29** 323
- [24] Schantz H G 2001 Electromagnetic energy around Hertzian dipoles *IEEE Ant. Propag. Mag.* **43** 50–62
- [25] Shamonina E, Kalinin V A, Ringhofer K H and Solymar L 2002 Short dipole as a receiver: effective aperture shapes and streamlines of the Poynting vector *IEE Proc. Microw. Antennas Propag.* **149** 153–9
- [26] Diao J and Warnick K F 2016 Poynting streamlines, effective area shape and the design of superdirective antennas *IEEE Trans. Antennas Propag.* **65** 861–6
- [27] Vallecchi A, Chu S, Solymar L, Stevens C J and Shamonina E 2019 Coupling between coils in the presence of conducting medium *IET Microw. Antennas Propag.* **13** 55–62
- [28] Guo Y, Li J, Hou X, Lv X, Liang H, Zhou J and Wu H 2017 Poynting vector analysis for wireless power transfer between magnetically coupled coils with different loads *Sci. Rep.* **7** 1–6
- [29] Liu Y and Hu A P 2018 Study of power flow in an IPT system based on Poynting vector analysis *Energies* **11** 165
- [30] Li W, Wang Q, Kang J and Wang Y 2020 Energy-concentrating optimization based on energy distribution characteristics of MCR WPT systems with SS/PS Compensation *IEEE Trans. Ind. Electron.* **67** 10410–20
- [31] Li W, Wang Q, Kang J and Wang Y 2019 Energy distribution characteristics of magnetically coupled resonant wireless power transfer systems considering four basic reactive power compensations *Prog. Electromagn. Res.* **86** 1–16
- [32] Wang H, Zhang C and Hui S Y R 2019 Visualization of energy flow in wireless power transfer systems *2019 IEEE Wireless Power Conf. (WPTC)* pp 536–41
- [33] Balanis C A 2016 *Antenna Theory: Analysis and Design* 4th edn (New York: Wiley)
- [34] Neumann F E 1846 Allgemeine Gesetze der inducirten elektrischen Ströme *Ann. Phys.* **143** 31–44

- [35] Zhuromskyy O, Sydoruk O, Shamonina E and Solymar L 2009 Slow waves on magnetic metamaterials and on chains of plasmonic nanoparticles: driven solutions in the presence of retardation *J. Appl. Phys.* **106** 104908
- [36] Tatartschuk E, Gneiding N, Hesmer F, Radkovskaya A and Shamonina E 2012 Mapping inter-element coupling in metamaterials: scaling down to infrared *J. Appl. Phys.* **111** 094904
- [37] Tai C 1964 The optimum directivity of uniformly spaced broadside arrays of dipoles *IEEE Trans. Antennas Propag.* **12** 447–54
- [38] Shamonina E and Solymar L 2015 Maximum directivity of arbitrary dipole arrays *IET Microw. Antennas Propag.* **9** 101–7
- [39] Vendik O G 1962 Determination of a mutual inductance between antennas on the known radiation patterns in Fraunhofer region *Radiotekhnika* **17** 11–18
- [40] Vendik O G and Yegorov Y V 2000 The first phased-array antennas in Russia: 1955–1960 *IEEE Antennas Propag. Mag.* **42** 46–52
- [41] Kalinin V, Solymar L and Shamonina E 2019 Kramers-Kronig relations for magnetoinductive waves *Phys. Rev. B* **100** 115130